Biogeochemistry (2011) 104:237–249
DOI 10.1007/s10533-010-9498-2

Subcellular localization of silicon and germanium in grass root and leaf tissues by SIMS: evidence for differential and active transport

Jed P. Sparks · Subhash Chandra · Louis A. Derry · Mandayam V. Parthasarathy · Carole S. Daugherty · Rory Griffin

Received: 10 December 2008 / Accepted: 16 June 2010 / Published online: 8 July 2010

Abstract Silicon transport and incorporation into plant tissue is important to both plant physiological function and to the influence plants have on ecosystem silica cycling. However, the mechanisms controlling this transport have only begun to be explored. In this study, we used secondary ion mass spectrometry (SIMS) to image concentrations of Si in root and shoot tissues of annual blue grass (*Poa annua* L.) and orchard grass (*Dactylis glomerata* L.) with the goal of identifying control points in the plant silica uptake pathway. In addition, we used SIMS to describe the distributions of germanium (Ge); the element used to trace Si in biogeochemical studies. Within root tissue, Si and Ge were localized in the suberized thick-walled region of endodermal cells, i.e. the proximal side of endodermal cells which is in close association to the casparian strip. In leaves, Si was present in the cell walls, but Ge was barely detectable. The selective localization of Si and Ge in the proximal side of endodermal cell walls of roots suggests transport control is exerted upon Si and Ge by the plant. The absence of Si in most root cell walls and its presence in the cell walls of leaves (in areas outside of the transpiration terminus) suggests modifications in the chemical form of Si to a form that favors Si complexation in the cell walls of leaf tissue. The low abundance of Ge in leaf tissue is consistent with previous studies that suggest preferential transport of Si relative to Ge.

Keywords Silicon · Germanium · Casparian strip · Secondary ion mass spectrometry (SIMS) · High pressure freezing · Freeze-substitution

J. P. Sparks
Department of Ecology and Evolutionary Biology, Cornell University, Ithaca, NY 14853, USA

S. Chandra
Cornell SIMS Laboratory, Department of Earth and Atmospheric Sciences, Cornell University, Ithaca, NY 14853, USA

L. A. Derry (✉) · R. Griffin
Department of Earth and Atmospheric Sciences, Cornell University, Snee Hall, Ithaca, NY 14853, USA
e-mail: derry@cornell.edu

M. V. Parthasarathy · C. S. Daugherty
Plant Biology and Cornell Integrated Microscopy Center, Cornell University, Ithaca, NY 14853, USA

Introduction

The uptake and biomineralization of silicon by higher plants is an important process with impact both on the function and productivity of plants and the biogeochemical cycle of silicon. Silica (expressed as SiO_2) content in plant tissue has been implicated in several functions including resistance to disease and pathogens, structural support, and resistance to herbivory (Epstein 1999; Fauteux et al. 2005). There is extensive agronomic evidence for the relationship between silica

availability and yield in crop plants including rice, wheat, and maize (Raven 2003; Richmond and Sussmman 2003). A number of field studies have shown that plant uptake of Si can strongly influence ecosystem and regional level cycling and transport of silicon (Lucas et al. 1993; Alexandre et al. 1997; Meunier et al. 1999; Carnelli et al. 2001; Lucas 2001; Derry et al. 2005). Historically, the study of the Si cycle in terrestrial environments has primarily focused on the release of Si from mineral weathering and its' coupling to the carbon cycle (e.g., White and Brantley 1995). However, biological processes play an increasingly recognized role in the global Si cycle. Conley (2002) estimated biological Si cycling in the terrestrial environment to be 60–200 Tmol $year^{-1}$; compared to the 240 Tmol $year^{-1}$ estimated to be cycled in the marine environment (Conley 2002; Treguer et al. 1995). The annual biological turnover of Si in terrestrial environments is at least an order of magnitude higher than the global rate of silica release from weathering of silicate minerals [5–8 Tmol $year^{-1}$ (Berner and Berner 1996)]. Understanding the role of biological cycling of silica in soil-forming processes and in controlling stream and soil water chemistry is a significant challenge in biogeochemistry. Here we present evidence from secondary ion mass spectrometry (SIMS) on the mechanisms controlling uptake of silicon and its analog element germanium by common grasses. We seek to improve understanding of the controls on Si and Ge uptake and possible fractionation in higher plants.

Silica occurs in nearly all plants. The amount of silica contained in tissues varies significantly (0.1–10% dry weight) depending upon the species (Epstein 1999). This strongly implies some level of control is exerted by the plant on the magnitude of silica taken into plant tissues. Previous work has shown plant roots take up silicon in the form of silicic acid (Raven 2003) and silicon is translocated through the plant as monomeric silicic acid (Casey et al. 2001; Mitani et al. 2005). Silica in plants is commonly found as amorphous silica bodies known as phytoliths but other forms are known. Post-harvest analyses have described polymers of hydrated amorphous silica in plant cell walls and silica-cellulose layers on the surface of leaves and stems (Yoshida et al. 1969).

Recent work has used the germanium–silicon ratio as a tracer of silica sources in the environment. Like silicon, germanium is a Group IVb element, with an ionic radius in the IV-coordinated state of 39 pm compared to Si = 26 pm (Shannon, 1976). Germanate structural analogs appear to form ideal solid solutions with silicate minerals (Capobianco and Navrotsky 1982; Martin et al. 1996; Evans and Derry 2002). Under most biogeochemically relevant conditions Ge is mainly present in the dissolved form as monomeric germanic acid ($Ge(OH)_4$), similar to silicic acid ($Si(OH)_4$) (Pokrovski and Schott 1998). In most silica-containing materials Ge is present at trace concentrations, with Ge/Si ratios typically from 0.2 to 5 μmol/mol in common minerals and natural waters (Mortlock and Froelich 1987). The similarity in oxidation state, crystal radii, hydration shell, and distribution between common minerals and the aqueous phase suggest that Ge may be useful as an analog for Si in biogeochemical studies. Early workers used the radioisotope ^{68}Ge to trace uptake of Si in plants and diatoms [Azam and Volcani 1981]. The use of stable Ge as a "pseudo-isotope" of silicon was pioneered as a tracer of the marine silica cycle (Froelich et al. 1985). Ge is not significantly fractionated from Si during uptake by diatoms, but is fractionated during weathering and hydrothermal processes (Froelich et al. 1992; Kurtz et al. 2002; Murnane and Stallard 1990; Evans and Derry 2002).

Field and laboratory studies indicate that leaf phytoliths isolated from a variety of plant groups have low Ge/Si relative to co-existing soil minerals or solutions (Derry et al. 2005, Garvin 2006; Blecker et al. 2007; Delvigne et al. 2009). Ge and Si distributions in two prairie grasses (*Agropyron smithii* and *Schizachyrium scoparium*) suggested that roots were the site of discrimination against Ge (Blecker et al. 2007). These observations support the use of Ge/Si ratios as a tracer of biogenic Si cycling in the terrestrial environment (Derry et al. 2005). However, fine-scale hydroponic measurements of Si and Ge absorption in wheat (Rains et al. 2006) and ^{68}Ge radio-isotope studies (Nikolic et al. 2007) have suggested Si and Ge compete with each other equally during root uptake. There appears to be some degree of uncertainty concerning the importance of fractionation between Ge and Si during plant uptake and biomineralization. While the use of Ge/Si ratios as a tracer of biogeochemical cycling of Si is promising, an improved understanding of the mechanisms and controls on any such fractionation is necessary to properly interpret field data.

Si concentrations in plants tend to be highest in leaves, implying that silica precipitation is commonly associated with the end of the transpiration stream, although silicification does occur in other tissues. Amorphous silica (opal) bodies in plant leaves (phytoliths) are widespread in plants and, after the decomposition of plant material, found in many soils. While there is a large body of evidence supporting the importance of silica in many plant groups, the mechanisms of silica uptake and biomineralization in plants are still not well understood. To date, most work on silica biomineralization has focused on siliceous plankton; significant progress has been made describing the genetic and biochemical controls in the marine diatom *Cylindrotheca fusiformis* (Hildebrand et al. 1997; Kroger et al. 2002; Perry 2003). However, similar progress has not been forthcoming in higher plants. Recently, Ma et al. (2006, 2007) described silica transporter genes in rice (Lsi1 and Lsi2) and their expression and localization were characterized by immunohistological fluorescence staining. The responsible genes appear to be related to those known to code for aquaporins and are not closely related to the genes responsible for silica transport in diatoms. Lsi1 was expressed on the distal side of both the exodermis and endodermis in rice roots, and is proposed to be responsible for symplastic Si transport into the endodermis (Ma et al. 2006). Lsi2 was expressed on the proximal side of both the exodermis and endodermis, and is proposed to be a Si efflux transporter (Ma et al. 2007). This combination of influx and efflux transporters in endodermis is proposed to be responsible for the effective transcellular transport of Si (Ma et al. 2007). The relationship between silica distributions in plant roots and the activity of the proposed transporters remains unclear. The most direct measurement would be to describe the distribution of silica within the plant at high resolution and fidelity. Scanning electron microscopy with X-ray microanalysis has been used with some success (Rafi et al. 1994). However, no method to date has been applied that describes the subcellular localization of silica and germanium within plants with high fidelity.

We investigated the subcellular location of silica and germanium in the common annual blue grass (*Poa annua* L.) and orchard grass (*Dactylis glomerata* L.) using dynamic SIMS based technique of ion microscopy. The goal was to determine spatial patterns and gradients potentially relevant to understanding uptake and biomineralization processes in the root and shoot tissues. Ion microscopy is ideally suited to this kind of study as it is capable of providing spatially resolved 3-D imaging of any elements from hydrogen to uranium with high sensitivity (ppm to ppb) and 500 nm spatial resolution (Castaing and Slodzian 1962; Linton and Goldsmith 1992; Chandra et al. 2000; Chandra 2005, 2008). Used in this mode the SIMS instrument provides high spatial resolution but only semi-quantitative data on concentrations, since emissivity factors for the different element have not been quantified in this matrix.

SIMS is a high vacuum technique and cryogenic sample preparations are needed for maintaining the chemical integrity of the sample. In the present study, we used high pressure freezing and freeze-substitution of grass tissues to study the localization of Si and Ge in common grass species with the explicit goals of identifying (1) control points in the plant silica uptake pathway, and (2) distributions of Si and Ge indicative of differential uptake.

Materials and methods

Plant tissue and growth conditions

Plants used in this study were grown hydroponically in a controlled growth facility located at Cornell University. Twenty-five individuals of annual blue grass (*Poa annua* L.) and canary grass (*Dactylis glomerata* L.) were germinated in perlite, allowed to grow for one week and then transferred to a commercial 80-L hydroponic system (Model 91003, American Hydro). The growth solution included a complete standard nutrient compliment (Hoagland solution) and amended with Si and Ge to initial concentrations of 0.5 mmol/L Si and 2 nmol/L Ge, for an initial Ge/Si $= 4 \times 10^{-6}$ mol/mol. Si was obtained from the dissolution of sodium metasilicate in distilled water, and Ge from an analytical standard solution in 2% HNO_3. These concentrations of Si and Ge are comparable to the higher end of natural soil solutions. The nutrient solution was changed weekly. Daytime temperature and light conditions were maintained at 25°C and 1000 μmol m^{-2} s^{-1}, respectively, throughout the period of growth. Nighttime temperatures were maintained at 20°C.

High pressure freezing and freeze-substitution

High-pressure freezing (Dahl and Staehelin 1989) and freeze-substitution in diethyl ether (Harvey et al. 1981) were used for optimal structural and chemical preservation of grass tissues in the study. One to 2 mm grass root and leaf (shoot) segments were cut with a razor blade and quickly transferred to a bath containing 0.03 M PIPES buffer (1,4 peprazinediethanesulfonic acid) plus 200 mM sucrose prior to freezing in a Balzer's HP10 High Pressure Freezer. The tissue samples were freeze-substituted in diethyl ether (DEE) at −90°C for 6 days. The 6-day substitution time was chosen based on the relatively long substitution time required for DEE, which is known for good preservation of intracellular chemical distribution. The tissue samples were then gradually warmed and embedded in Spurr's low viscosity resin.

Light microscopy analysis of freeze-substituted samples

One-micron thick sections that were stained in Azure blue were used for light microscopy analysis for morphological observations.

Sectioning and mounting of freeze-substituted samples for spatially resolved chemical analysis with SIMS ion microscopy

Sections of ~1 μm thickness that were obtained from the freeze-substituted samples were either collected on water or picked up dry before mounting them as flat as possible on polished tantalum substrates for SIMS analysis. Tantalum is an electrically conducting substrate that does not interfere with the analysis of the elements of interest in the present study and provides a smooth surface for SIMS analysis (the sample is held at ±4500 V relative to ground in the ion microscope instrument).

SIMS imaging of elemental (isotopic) distributions in grass root and shoot tissues

A dynamic SIMS CAMECA IMS-3f ion microscope instrument capable of producing isotopic images with 500 nm spatial resolution was used in this study (Chandra et al. 2000). Over its lifetime, the instrument has been upgraded and is equipped with a primary beam mass filter and a 5f Hall Probe control chassis. The control system of the instrument has also been upgraded with a Charles Evans and Associates model PC-1CS Computer Interface system with a Windows-based computer. A 5.5 keV mass filtered primary ion beam of O_2^+ was raster scanned over either 250 or 500 μm^2 regions of the sample for imaging studies. A 60 μm contrast aperture and either 150 or 400 μm transfer optics were employed in the imaging mode for the detection of positive secondary ion signals. The primary ion beam intensity was adjusted to 200 nA (250 μm^2 raster) for 150 μm transfer optics and 600 nA (500 μm^2 raster) for 400 μm transfer optics for the analysis of 1 μm thick freeze-substituted sections mounted on the tantalum substrates. SIMS images with masses 23, 28, 29, 39, 40, and 72 revealed the distribution of ^{23}Na, ^{28}Si, ^{29}Si, ^{39}K, ^{40}Ca, and ^{72}Ge isotopes, respectively, in the tissue. Both ^{28}Si and ^{29}Si isotopes were imaged to confirm the distribution of silicon in tissue structures. The germanium distribution was studied at mass 72 ($^{72}Ge^+$) which revealed significantly higher purity of the secondary ion signals as compared to the major isotope ^{74}Ge in this sample matrix.

SIMS isotope images were digitized directly from the microchannel plate/fluorescent screen assembly of the ion microscope using a slow scan charge-coupled device (CCD) camera (Photometrics; Tucson, AZ; Model CH220 CCD liquid-cooled camera head equipped with a Thomson-CSF TH7882 CDA CCD) and digitized to 14 bits per pixel with a Photometrics camera controller. The composite photographs showing multi-elemental (isotopic) distributions in designated tissues were made in Photoshop® from individual SIMS images recorded with the CCD camera.

Results

Light microscopy analysis of high pressure frozen and freeze-substituted grass tissues

Figure 1 shows light microscopy observations of structural details in high pressure frozen and freeze-substituted root (Fig. 1a) and shoot (Fig. 1b) tissues. Typical morphological features of distinct layers of

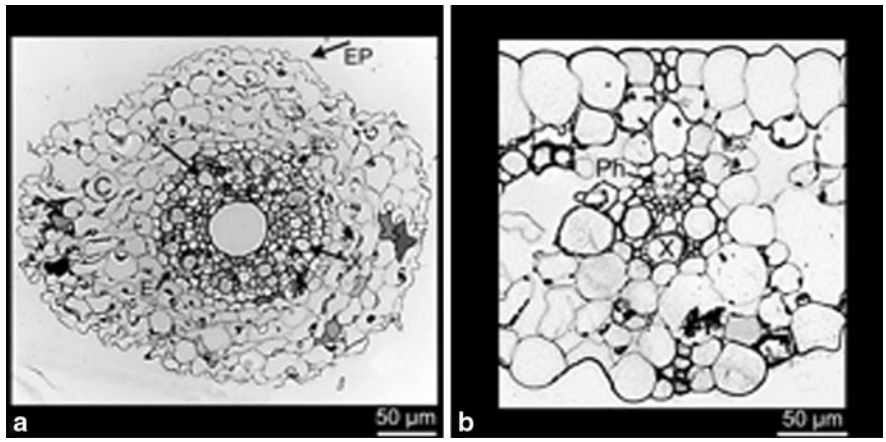

Fig. 1 Light micrographs showing morphological preservation in high pressure frozen and freeze-substituted root and shoot tissues of annual blue grass (*Poa annua* L.). Similar preservation was observed in orchard grass (*Dactylis glomerata* L.). The root epidermis (EP), the large, highly vacuolate cortical cells (*C*) are discernible, along with the distinct layer endodermis (*E*) that separates the cortical tissue from the vascular cylinder (**a**). Vascular tissues, xylem (*X*) and phloem, and parenchyma cells of pith are also well preserved (**a**). Similarly, well-preserved structural features are also seen in the shoot (leaf) tissue (**b**). The xylem vessels (*X*) and phloem (*Ph*) are identified with letters and *arrows* (**b**)

cells are discernible in both tissues. The root epidermis (EP), the large, highly vacuolate cortical cells (C), and the distinct layer endodermis (E) that separates the cortical tissue from the vascular cylinder are all visible in the image (Fig. 1a). Vascular tissues, xylem (X) and phloem, and parenchyma cells are also visible (Fig. 1a). Similarly, well-preserved structural features are evident in the leaf tissue (Fig. 1b). Individual cells in the epidermis and parenchyma are distinct. Xylem vessels (X), phloem (Ph), and individual cells of the lower epidermis can be easily identified.

SIMS imaging of subcellular distributions of Ca, Si, Ge, K, and Na in root tissue

We imaged ^{29}Si and ^{72}Ge for the direct comparison of the spatial distributions of Ge and Si. ^{40}Ca was imaged because Ca a major component of cell walls and thus gives a good image of the cellular structure by SIMS. Because preparation of biological tissues for microsectioning can disturb elemental distributions, ^{39}K, and ^{23}Na were imaged as a test of the fidelity of sample preservation (Chandra et al. 2000, Chandra 2005, discussed further below). Figure 2 is a composite photograph showing positive secondary ion SIMS images of ^{40}Ca, ^{29}Si, ^{72}Ge, ^{39}K, and ^{23}Na isotopic distributions in designated panels (Fig. 2a–e) from a 1 µm thick section of root tissue. SIMS images represent spatially resolved distribution of the total concentration of designated elements, via the detection of their respective major (or minor) isotopes, and the relative sensitivity of SIMS detection can vary between different elements. The level of brightness within a SIMS image is proportional to the relative concentration of the analyte in spatially resolved regions. The rarer ^{29}Si isotope (4.7% atom abundance) is shown in this image. In the ^{40}Ca SIMS image (Fig. 2a), the root-tissue structure is discernible as calcium is a major component of the cell walls. The major histological features of the root, such as the epidermis, cortical cells, and large parenchyma cells are distinguishable from the distinct inner layers of cells in the endodermis. Since SIMS images are formed from a gradual sputtering (ablation) of the sample surface in the Z-direction (i.e., downward into the surface of the sample), the distributions of silicon, germanium, potassium and sodium can be revealed in the same tissue (Fig. 2b–e).

The SIMS images of silicon and germanium (Fig. 2b, c) show a highly localized pattern of distribution in the root tissue. Silicon and germanium are both localized at the exterior of the vascular cylinder. This general region is often referred to as the casparian strip and is characterized by thickened and highly suberized cell walls and a point of

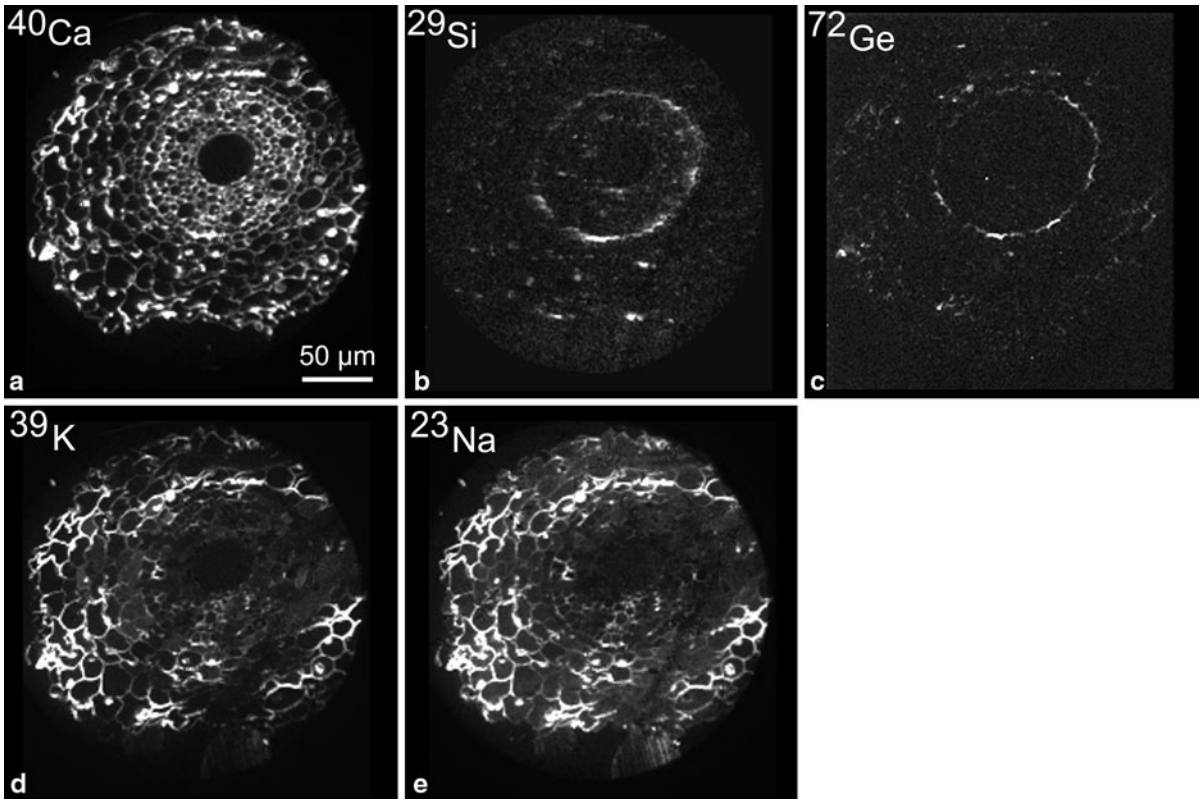

Fig. 2 Subcellular SIMS imaging of the positive secondary ions of ^{40}Ca, ^{29}Si, ^{72}Ge, ^{39}K, and ^{23}Na isotopes in high pressure frozen and freeze-substituted root tissue of annual blue grass (*Poa annua* L.). Similar preservation was observed in orchard grass (*Dactylis glomerata* L.). The level of brightness in individual SIMS images shown in designated *panels* (**a**–**e**) reveal the gradient of the designated isotope (element) in the tissue. The image integration times on the CCD imager for SIMS images were 60 s for the ^{40}Ca image, 2 min each for ^{29}Si and ^{72}Ge images, and 5 s each for ^{39}K, and ^{23}Na images

symplastic-only transport. Silicon and germanium signals are localized in the cell wall of the endodermal cells (Fig. 2b, c).

The ^{39}K and ^{23}Na distributions are similar and differ from the ^{40}Ca distribution in the root tissue (Fig. 2). These images are representative of distributions of these elements found in the root tissue in five replicates of each species regardless of the wet and dry sectioning methods for collecting sections.

Figure 3 shows a higher magnification view of a root cross section. In this image, the more common ^{28}Si isotope (natural abundance 92.3%) is shown. The four images were generated sequentially [i.e., the first ^{40}Ca SIMS image shown in pseudo-color green (Fig. 3a) was recorded prior to the ^{28}Si (red) and ^{72}Ge image (blue) (Fig. 3b, c)]. The ^{28}Si and ^{72}Ge SIMS images again show the accumulation of Si and Ge in the endodermal cell walls. In order to test that the SIMS 3-D sampling did not completely remove the tissue structures during this analysis, a second ^{40}Ca image (shown in grayscale) (^{40}Ca-2, Fig. 3d) was recorded after the recording of the ^{72}Ge image. The second ^{40}Ca image clearly matches the first ^{40}Ca image confirming the SIMS sampling of both ^{28}Si and ^{72}Ge images in tissue material in between the two calcium images is a representation of the true localization and not from any ion microscopic sampling errors during analysis. The overlay and superimposition of ^{28}Si (red) and ^{72}Ge (blue) SIMS images over the ^{40}Ca-1 (green) image is shown in panel "e" (Fig. 3e) to illustrate an unequivocal co-localization of Si and Ge in the same subcellular region of endodermal cells. A magnified view of a portion of the overlay demonstrates that both Si and

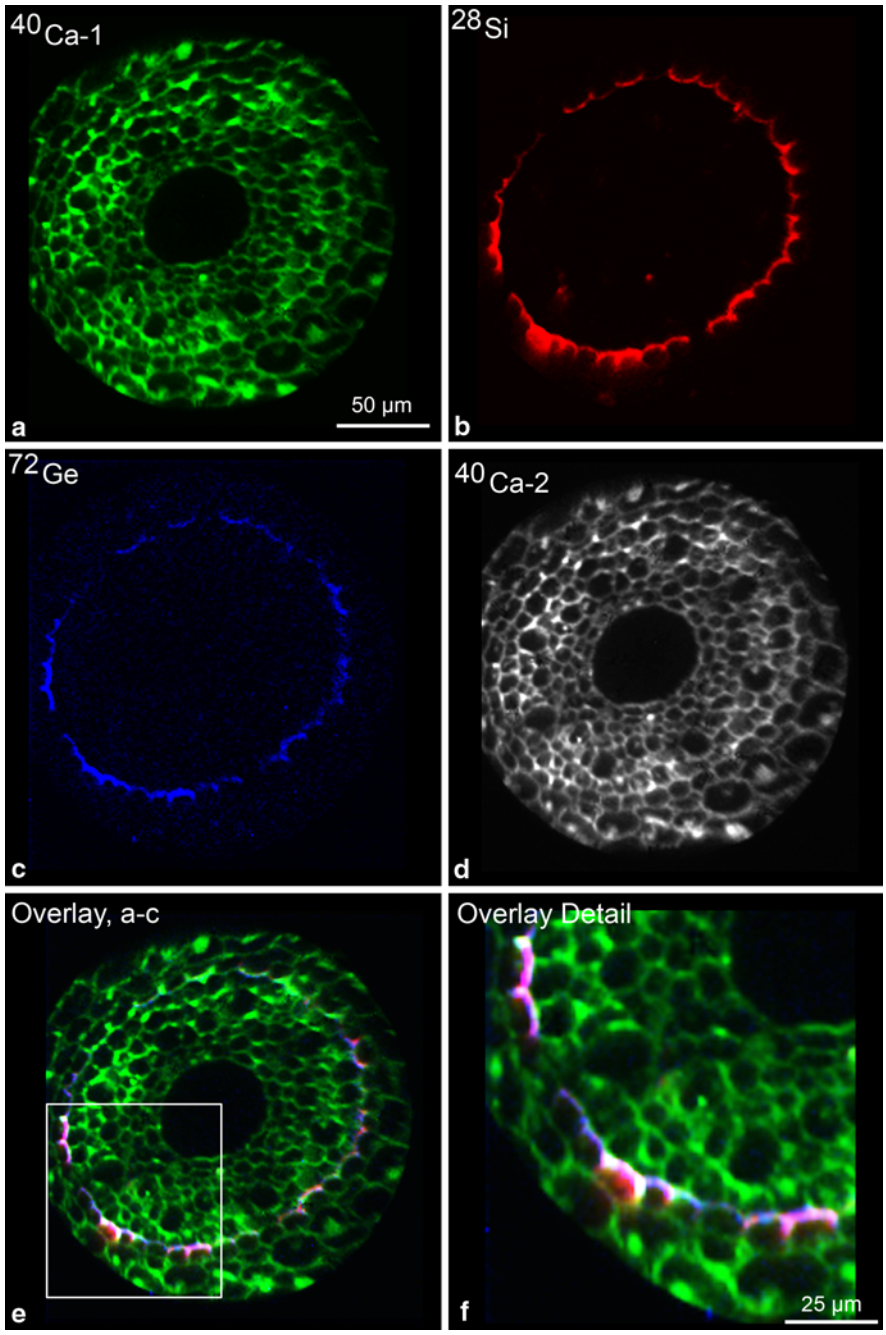

Fig. 3 Three-dimensional subcellular SIMS imaging of the positive secondary ions of ^{40}Ca, ^{28}Si, ^{72}Ge, and ^{40}Ca isotopes in high pressure frozen and freeze-substituted root tissue of the annual blue grass (*Poa annua* L.). Similar preservation was observed in orchard grass (*Dactylis glomerata* L.). The images of ^{28}Si and ^{72}Ge were recorded between the two ^{40}Ca images (^{40}Ca-1 and ^{40}Ca-2) shown in designated *panels* (**a**–**d**). The pseudo-colors and overlay displays illustrate co-localization of Si and Ge in proximal cell walls of endodermal cells (**e**, **f**). The image integration times on the CCD imager for SIMS images were 1 min each for ^{40}Ca images, 30 s for the ^{28}Si image, and 2 min for the ^{72}Ge image. *Note*: In printed copy of the journal, all color images in this figure are shown as black-and-white images. This does not change the overall interpretation of the data that both Si and Ge are co-localized in the proximal side of endodermal cells in the root

Ge localize in the proximal side of endodermal cell walls (Fig. 3f).

A light microscope image of the same tissue (Fig. 4) shows the structure in which Si and Ge are localized. Both Si and Ge occur in the proximal side of endodermal cell walls (PE, indicated by arrows in Fig. 4), in a close association to the well known location of Casparian strip.

SIMS imaging of subcellular distributions of Ca, Si, Ge, K, and Na in leaf tissue

Figure 5 is a composite photograph showing positive secondary ion SIMS images of ^{40}Ca, ^{28}Si, ^{72}Ge, ^{39}K, and ^{23}Na isotopic distributions in designated panels (Fig. 5a–e) from a 1 µm thick section of the leaf tissue. Calcium is localized in cell walls with some

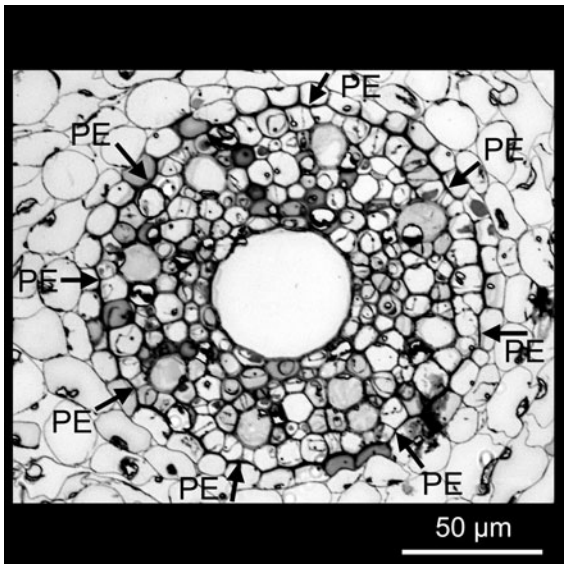

Fig. 4 Light microscopy image from a 1-µm thick section from the tissue adjacent to the one used for SIMS imaging in Fig. 3. The *arrows* identify the proximal side of endodermal cells (PE) as the primary site for Si and Ge localization in the previous SIMS images

degree of heterogeneity and with a higher accumulation in the primary epidermal cell wall (Fig. 5a). Leaf trichomes also contain calcium (top left area of the image). Silicon is not preferentially localized in any particular cell type and is associated with the cell walls in much of the leaf tissue (Fig. 5b). Germanium, at barely detectable concentrations, is associated with cell walls (Fig. 5c). The ^{39}K and ^{23}Na distributions suggest these elements do not concentrate in leaf trichomes (Figs. 5d and 5e), but are localized in the parenchyma cells and the cells of the lower epidermis.

Due to the presence of Na^+–K^+-ATPase in the plasma membrane of eukaryotic cells, the preservation of higher levels of intracellular potassium than sodium has been used as a criterion for SIMS evaluation of the reliability of sample preparation in animal cells (Chandra et al. 2000, Chandra 2005). However, the specialized plant structures implicated with the transport of elements and the presence of large vacuoles in plant cells make it difficult to observe high K-low Na intracellular signals in all cells. Despite these complexities, there is still some validation of this criterion as shown in individual cell images of ^{39}K and ^{23}Na distributions shown in Fig. 5 (indicated by arrows). In this analysis, the image integration times on the CCD camera were identical for ^{39}K and ^{23}Na. Since the SIMS' relative sensitivity factors are comparable for ^{39}K and ^{23}Na in the plant tissues (Ramseyer and Morrison, 1983), we calculated $^{39}K^+/^{23}Na^+$ ratios from SIMS images in individual cells. Interestingly, the observed $^{39}K^+/^{23}Na^+$ ratio of $\sim$10 in these cells is in general agreement to the ratios of these elements typically observed in animal and plant cells (Chandra et al. 2002; Chandra 2005; Derue et al. 2006).

The ratio of $^{72}Ge^+/^{28}Si^+$ secondary ions was calculated for the proximal side of endodermal cells walls of the root tissue and cell walls in the leaf tissue after pixel-by-pixel registration of $^{28}Si^+$ and $^{72}Ge^+$ SIMS images for spatial correlation (e.g. Figs. 3, 5). Because SIMS relative sensitivity factors (RSF) for $^{28}Si^+$ and $^{72}Ge^+$ are not known in this sample type, this ratio is only semi-quantitative. While the absolute intensities or ratios we obtained cannot be used to quantify Ge or Si concentrations, the $^{72}Ge^+/^{28}Si^+$ ratios can be compared among our samples since the sample matrix does not appear to differ greatly. The observed $^{72}Ge^+/^{28}Si^+$ in the leaf tissue is 2–3 times lower than in the proximal cell wall regions of the root, where the measured Ge and Si are outside the xylem stream. The depletion of Ge in leaf tissues relative to Si of factor of 2–3 is similar, but somewhat less, than that reported from bulk analyses of grasses in laboratory and field experiments (Blecker et al. 2007; Delvigne et al. 2009). Those authors found depletion of Ge of a factor of 5 or greater between the growth medium and the shoot tissue. The difference may reflect a different basis for comparison, as well as the higher RSF for Ge relative to Si. If we apply the RSF(Ge/Si) = 3.0 determined by Wilson (1995) our results are in reasonable quantitative agreement with those of Blecker et al. (2007) and Delvigne et al. (2009). The Blecker et al. and Delvigne et al. studies compared bulk leaf tissue to growth solutions, while the present study compares microanalysis of leaf cell wall material to the silica rich regions around the casparian strip in the proximal side of cell walls of the root endodermal cells. In any case the direction is the same, and the magnitude comparable, implying that transport across the endodermal cell layer (and casparian strip) to the xylem stream is an important step in fractionating Ge from Si in higher plants.

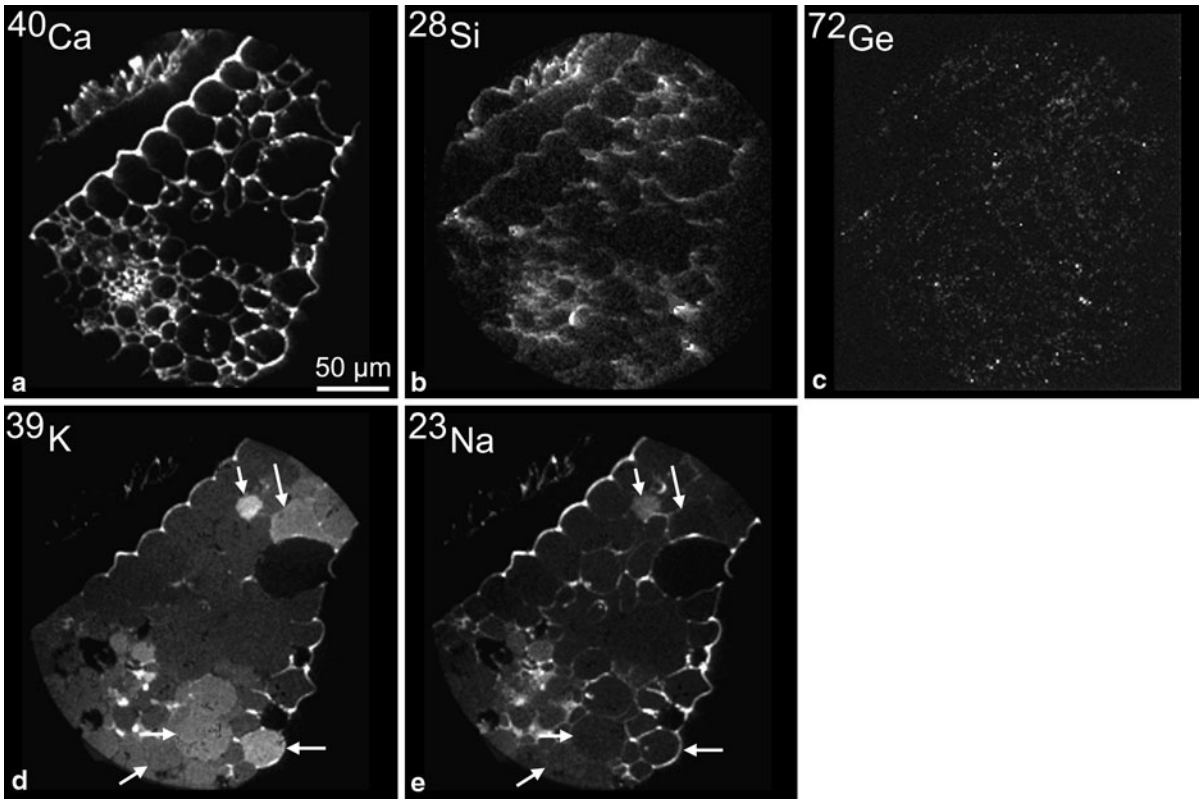

Fig. 5 Subcellular SIMS imaging of the positive secondary ions of ^{40}Ca, ^{28}Si, ^{72}Ge, ^{39}K, and ^{23}Na isotopes in high pressure frozen and freeze-substituted leaf (shoot) tissue of the annual blue grass (*Poa annua* L.). Similar preservation was observed in orchard grass (*Dactylis glomerata* L.). The level of brightness in individual SIMS images shown in designated *panels* (**a**–**e**) reveal the gradient of the designated isotope (element) in the tissue. The *arrows* point to individual cells with high ^{39}K-low-^{23}Na signals. The image integration times on the CCD imager for SIMS images were 60 s for the ^{40}Ca image, 2 min each for ^{28}Si and ^{72}Ge images, and 5 s each for ^{39}K, and ^{23}Na images

Discussion

To the best of our knowledge, the present manuscript is the first attempt to analyze Si and Ge at subcellular scale resolution with SIMS in grass tissues. There is no available literature for assessing the detection limits of these elements in freeze-substituted sample type. It should be noted that the SIMS sensitivities of these elements do not affect a comparison of the ratio between different SIMS images since the comparison is limited to the cell wall matrix in the present study. Future work is needed in this area for quantification of SIMS images. However, in materials samples, the detection limits for Si and Ge were observed to be in the low ppm range for the type of SIMS instrument used in the present study (Tanaka et al. 1988).

Our SIMS observations indicate that Si and Ge clearly accumulate in the cell walls of endodermal cells (Figs. 2, 3). This implies some level of exclusion of both Si and Ge by the casparian strip. A likely scenario is that transport becomes symplastic at the edge of the vascular cylinder, silica and germanium are actively transported at some rate less than that for the bulk flow of water causing Si and Ge to come out of solution and deposit locally to the cell wall. The distribution of Si and Ge in the proximal side of cell walls of endodermal cells is in very close agreement with the localization of silica transporter gene Lsi2 (Ma et al. 2007) in rice. Lsi2 was reported to be expressed on the proximal side of plasma membranes of cells in the endodermis, and is proposed to be a Si efflux transporter into the stele (Ma et al. 2007). The present study provides the first direct evidence that a gradient of Si and Ge is also present in identical subcellular location of endodermal cells in grass roots. Based on a very limited data set that showed a

single root phytolith with low Ge/Si, Blecker et al. (2007) suggested that Ge was excluded from the root at the root-solution interface. However Delvigne et al. (2009) showed that the root tissues of banana (*Musa*) and horsetails (*Equisetum*) had high Ge/Si, while tissues further along the transpiration stream had much lower Ge/Si. They suggested an alternative hypothesis that plant uptake did not discriminate against Ge, but rather that Ge preferentially accumulated in the root zone, resulting in relative depletion of Ge in tissues further down the transpiration stream. Our study appears broadly consistent with this conclusion. Delvigne et al. further suggest that Ge might be stored in roots as organic complexes. However we found that silica-rich bodies along the proximal side of endodermal cell walls sequester Ge, and did not observe any evidence for accumulation of Ge at sites not associated with silica. These observations suggest that Ge may indeed accumulate in root zones, but is most likely associated with silica in biogenic opal rather than stored as organic complexes.

Ge and Si transport

It seems extremely unlikely the observed pattern of Si and Ge could result from simple diffusive transport, and is consistent with the suggestion of active transport of silicon in plant roots (Tamai and Ma 2003; Ma et al. 2006, 2007).

In the shoots, we find that Si is localized in most cell walls (Fig. 5). In contrast, Ge is very low to undetectable throughout the leaf. This information combined with the evidence for controlled transport within the roots (Figs. 2, 3) suggests the transport of Si and Ge may be fundamentally different. Whole-leaf digestion data from many plant leaves show low Ge/Si relative to growth water (Derry et al. 2005; Garvin 2006; Blecker et al. 2007) and suggest large fractionations against Ge relative to Si are common during plant uptake. The recent work of Delvigne et al. (2009), where they found low $(Ge/Si)_{leaf}$ relative to soil solutions in field-grown bananas and horsetails, is in excellent agreement with these studies, This is in contrast to fine-scale root uptake studies using the radiotracer ^{68}Ge (Rains et al. 2006). The data we present here supports a discrimination against Ge compared to Si. Why there is disagreement among these sources is unclear. Studies supporting a discrimination tend to come from field comparisons of solution to biomass Ge:Si or laboratory studies (like the one presented here) where Ge and Si within the growth solution mimics natural soil concentrations. Studies reporting similar uptake tend to use equivalent Si and Ge concentrations in the growth solution, with Ge/Si ratios 5 to 7 orders of magnitude greater than known natural growth environments (Rains et al. 2006). It seems likely that such enormous perturbation of Ge levels in the growth medium fundamentally changes the uptake dynamic between the two elements. However, recently Nikolic et al. (2007) reported both root and shoot Ge/Si similar to the growth medium even when using a growth solution with ^{68}Ge concentrations comparable to Ge in natural soil solutions, and concluded that there was no significant discrimination between Ge and Si during uptake. Nikolic et al. do not provide uncertainties in their paper, but taken at face value their data indicate, on average, about a 5% *preferential uptake* of Ge in both root and shoot tissues relative to the nutrient solution. This result is in the opposite sense to our work and that of Delvigne et al. (2009) and also opposite to the modest discrimination against Ge that would be expected from passive diffusion alone (see below). The reasons for the discrepancy between the Nikolic et al. ^{68}Ge technique that shows little or no fractionation and the ICP-MS data of Blecker et al. and Delvigne et al. that show large fractionations are not clear, although the assumption that the radiotracer will behave quantitatively in the same way as natural trace elements is not clear because of potential difficulty with isotopic equilibration with the sample and short-lived radiotracer. One other possibility is that the dry ashing technique at 550°C used by Nikolic et al. promoted volatilization of Ge–F or Si–F complexes, a phenomenon we have observed in some samples (for this reason our lab uses a closed system microwave wet digestion at much lower $T = 180$°C). Regardless, this evident discordance in results deserves further investigation.

Passive vs active mechanisms of Ge–Si fractionation

The accumulation of Si and Ge around the casparian strip (Fig. 3) sets up a significant chemical gradient which could drive diffusive transport. Differences in the diffusivity of Si and Ge could contribute to the

observed fractionation. Si and Ge are present almost exclusively as silicic acid $Si(OH)_4$ and the homologous germanic acid $Ge(OH)_4$ at pHs typical of soil and plant roots (Pokrovski and Schott 1998). The diffusivity D of uncharged species can be estimated from the Stokes–Einstein equation:

$$D = \frac{k_B T}{6\pi\mu R_o} \quad (1)$$

where k_B is the Boltzman constant, T is temperature, μ is the kinematic viscosity of the solvent, and R_o is the effective radius of the solute molecule. The absolute accuracy of the Stokes–Einstein equation has been the subject of discussion in the literature (Edwards 1970; Cussler 1997). Here we are only concerned with relative differences in diffusivity, for which it is quite likely to be sufficiently robust for our purposes. Consequently the parameter of interest is R_o, typically estimated with van der Waals radii. However the van der Waals radius of Ge is not well known (Bondi 1964). Instead we compare the Si–O and Ge–O bond distances (Shannon and Prewitt 1969). The geometry of the $Si(OH)_4$ molecule given by Gibbs et al. (1994) suggests that these bond lengths should closely approximate the molecular radius. The Si–O distance is 160.7 pm, while Ge–O is 173.8 pm. For $\mu_{H_2O} = 0.1$ g cm^{-1} s^{-1} and $T = 298$ K the Stokes–Einstein equation predicts $D_{Si} = 1.36 \times 10^{-5}$ cm^2 s^{-1}, while $D_{Ge} = 1.25 \times 10^{-5}$ cm^2 s^{-1}, a difference of only 7.6%.

The fractionations observed in field studies (and presented here) are simply too great to be explained by molecular diffusion, or by the differences in the energetics of amorphous SiO_2 or GeO_2 precipitation (e.g. Pokrovski and Schott 1998). Thus, passive mechanisms seem incapable of producing such large fractionations ($\geq$5 $\times$ enrichment of Si over Ge in leaf tissues relative to source water). In contrast, active transport mechanisms in plants are known to be highly specific and it is not unreasonable to expect that active and plant-controlled transport could cause significant differential uptake of Ge and Si as germanic and silicic acids into the xylem. The silica transporter gene Lsi1 and Lsi2 reported from rice (Ma et al. 2006, 2007) are closely related to those known to code for aquaporins, "water channel" proteins implicated in the transport of small uncharged molecules such as water and glycerol. By analogy an aquaporin type protein may be well suited for the active transport of the small, uncharged silicic acid molecule. Specificity in terms of molecular radius and vibrational frequencies may be sufficient to significantly discriminate against low levels of natural Ge, but less effective when Ge levels are enriched by six orders of magnitude as used in some laboratory studies of Ge uptake. The observation in this study of the localization of both Si and Ge in the proximal side of endodermis of the plant root and the similar localization of the Lsi2 transporter gene made by Ma et al. (2007) strongly suggests active transport and that the transport mechanism discriminates against Ge. Differences in the transport efficiency for Ge and Si may shed light on the nature of the transport mechanism. We note that available evidence indicates that all higher plants analyzed to date, including examples of woody and herbaceous groups, and gymno- and angiosperms, show strong fractionation against Ge relative to Si, even when they accumulate very different levels of biogenic silica (Derry et al. 2005; Garvin 2006; Blecker et al. 2007; Delvigne et al. 2009). This widespread tendency to fractionate Ge from Si suggests that the mechanism responsible for Si transport during plant uptake may be common to many or all vascular plants.

We observed silicon in the cell walls of leaf tissue but not in the cell walls of root cells other than the endodermis (see Figs. 2, 3, 5). This suggests the chemical form of either silicon or the cell wall material itself is different in the shoot changing the affinity for the deposition of Si to the cell wall. This observation is consistent with the observation that silicon plays a significant role in the aboveground structure of many plants (e.g., Epstein 1999; Fauteux et al. 2005).

The sample preparation for plant cells has long remained an area of active research in SIMS and many approaches have been used including chemical fixation, freeze-substitution, freeze-drying, and frozen-hydrated samples (see, e.g. Linton and Goldsmith 1992; Lazof et al. 1996; Grignon et al. 1996; Derue et al. 2006). The choice for a particular method of sample preparation is problem- and sample type-dependent. For the present work, chemical analysis of cells and tissue structures of the root and leaf tissues were needed for understanding the localization and transport characteristics of Si and Ge in plants. This study shows that the freeze-substitution method coupled with high pressure freezing can provide a

valuable methodology for SIMS studies of elements in plant tissues. Although the preservation of structural details can be evaluated more precisely using TEM analysis of high pressure frozen tissues, the evaluation of localized and spatially resolved chemical composition is often more difficult. SIMS, with the appropriate sample preparation technique, appears to be a good method for such chemical analyses and the validity of sample preparation can be assessed using K/Na ratios.

Finally, this study demonstrates that SIMS imaging, following careful sample preparation, can be a powerful tool for studying the distribution and transport processes of a wide range of elements in plant tissues. Since stable isotopes can be used in plant experiments and imaged separately by SIMS (as shown by the imaging of ^{28}Si and ^{29}Si in Figs. 2, 3), rarer isotopes could be used as tracers with a multitude of applications. The ability to monitor isotopes at fine resolution within plant cells will enable novel approaches for understanding the kinetics of elemental uptake and the turnover of elements within cells and other tissue structures within plants. In the case of Ge and Si both spatially resolved but semi-quantitative and quantitative point SIMS analyses can be an important tool for understanding the mechanisms of elemental and isotopic fractionation in the solution-plant environment.

Acknowledgements This work was supported by a National Science Foundation Grant J. Sparks (DEB–0237674), Biological and Environmental Research Program (BER), U.S. Department of Energy, Grant No. DE-FG02-91ER61138 to S. Chandra, and the Research Experience for Undergraduates program (DMR-0097494) through the Cornell Center for Materials Research (CCMR). Partial financial support from Cornell Core Facilities and NYSTAR program to S. Chandra is also acknowledged. The technical help of Dena Vallano, Shannon Caldwell, Anita Alsuisio, and Kimberlee Sparks is gratefully acknowledged. Daniel Lorey is acknowledged for the use of Photoshop in making grayscale composite photographs. Joshua Abraham is acknowledged for the use of Photoshop in making the pseudo-color image composite shown in Fig. 3.

References

Alexandre A, Meunier J-D, Colin F, Koud J-M (1997) Plant impact on the biogeochemical cycle of silicon and related weathering processes. Geochim Cosmochim Acta 61: 677–682. doi:10.1016/S0016-7037(97)00001-X

Azam F, Volcani BE (1981) Germanium-silicon interactions in biological systems. In: Simpson TL, Volcani BE (eds) Silicon and siliceous structures in biological systems. Springer-Verlag, New York, pp 43–67

Berner EK, Berner RA (1996) Global environment: water, air, and geochemical cycles. Prentice Hall, Upper Saddle River, NJ, 376 p

Blecker SW, King SL, Derry LA, Chadwick OA, Ippolito JA, Kelly EF (2007) The ratio of germanium to silicon in plant phytoliths: quantification of biological discrimination under controlled experimental conditions. Biogeochemistry 86(2):189–199. doi:10.1007/s10533-007-9154-7

Bondi A (1964) van der Waals volumes and radii. J Phys Chem 68:441–451

Capobianco C, Navrotsky A (1982) Calorimetric evidence for ideal mixing of silicon and germanium in glasses and crystals of sodium feldspar composition. Am Mineral 67: 718–724

Carnelli AL, Madella M, Theurillat JP (2001) Biogenic silica production in selected alpine plant species and plant communities. Ann Bot 87(4):425–434

Casey WH, Phillips BL, Furrer G (2001) Aqueous aluminum polynuclear complexes and nanoclusters: a review. Nanoparticles and the environment. Rev Mineral Geochem 44:167–190

Castaing R, Slodzian G (1962) Microanalyse par emission ionique secondarie. J Microsc (Paris) 1:395–410

Chandra S (2005) Quantitative imaging of subcellular calcium stores in mammalian LLC-PK1 epithelial cells undergoing mitosis by SIMS ion microscopy. Eur J Cell Biol 84: 783–797

Chandra S (2008) Subcellular imaging of RNA distribution and DNA replication in single mammalian cells with SIMS: the localization of heat shock induced RNA in relation to the distribution of intranuclear bound calcium. J Microsc 232:27–35

Chandra S, Smith DR, Morrison GH (2000) Subcellular imaging by dynamic SIMS ion microscopy. Anal Chem 72:104A–114A

Chandra S, Kabalka GW, Lorey D R II, Smith DR, Coderre JA (2002) Imaging of fluorine and boron from fluorinated-boronophenylalanine in the same cell at organelle resolution by correlative SIMS ion microscopy and confocal laser scanning microscopy. Clin Cancer Res 8:2675–2683

Conley DJ (2002) Terrestrial ecosystems and the global biogeochemical silica cycle. Global Biogeochem Cycles 16:68(1)–68(8). doi:10.1029/2002GB001894

Cussler EL (1997) Diffusion: mass transfer in fluid systems. Cambridge University Press, Cambridge, p 580

Dahl R, Staehelin LA (1989) High-pressure freezing for the preservation of biological structures: theory and practice. J Electron Microsc Tech 13:165–174

Delvigne C, Opfergelt S, Cardinal D, Delvaux B, Andre L (2009) Distinct silicon and germanium pathways in the soil-plant system: evidence from banana and horsetail. J Geophys Res 114:G02013. doi:10.1029/2008JG000899

Derry LA, Kurtz AC, Ziegler K, Chadwick OA (2005) Biological control of terrestrial silica cycling and export fluxes to watersheds. Nature 433:728–731. doi:10.1038/nature03299

Derue C, Gibouin D, Demarty M, Verdus M-C, Lefbre F, Thellier M, Ripoll C (2006) Dynamic-SIMS imaging and quantification of inorganic ions in frozen-hydrate plant samples. Microsc Res Technol 69:53–63

Edwards JT (1970) Molecular volumes and the Stokes-Einstein equation. J Chem Educ 47:261–270
Epstein E (1999) Silicon. Annu Rev Plant Physiol Plant Mol Biol 50:641–664
Evans MJ, Derry LA (2002) Quartz control of high germanium/silicon ratios in geothermal waters. Geology 30: 1019–1022
Fauteux F, Remus-Borel W, Menzies JG, Belanger RR (2005) Silicon and plant disease resistance against pathogenic fungi. FEMS Microbiol Lett 249:1–6
Froelich PN, Hambrick GA, Andreae MO, Mortlock RA, Edmond JM (1985) The geochemistry of germanium in natural waters. J Geophys Res 90:1133–1141
Froelich PN, Blanc V, Mortlock RA, Chillrud SN, Dunstan W, Udomkit A, Peng T-H (1992) River fluxes of dissolved silica to the ocean were higher during the glacials: Ge/Si in diatoms, rivers, and oceans. Paleoceanography 7:739–768
Garvin CJ (2006) An exploratory study of the terrestrial silicon cycle at a small watershed in Northern Vermont. MS thesis, Cornell, Ithaca, New York, USA
Gibbs GV, Downs JV, Boisen MB Jr (1994) The elusive SiO bond. Rev Mineral 29:331–368
Grignon N, Halpern S, Jeusset J, Briancon C, Fragu P (1996) Localization of chemical elements and isotopes in the leaf of soybean (*Glycine max*) by secondary ion mass spectrometry microscopy: critical choice of sample preparation procedure. J Microsc 186:51–66
Harvey DMR, Hall JL, Flowers TJ, Kent B (1981) Quantitative ion localization within Suaeda meritima leaf mesophyll cells. Planta 151:555–560
Hildebrand M, Volcani BE, Gassmann W, Schroeder JI (1997) A gene family of silicon transporters. Nature 385:688–689
Kroger N, Lorenz S, Brunner E, Sumper M (2002) Self-assembly of highly phosphorylated silaffins and their function in biosilica morphogenesis. Science 298:584–586
Kurtz AC, Derry LA, Chadwick OA (2002) Germanium-silicon fractionation in the weathering environment. Geochim Cosmochim Acta 66:1525–1537
Lazof DB, Goldsmith JG, Rufty TW, Linton RW (1996) The early entry of Al into cells of intact soybean roots: a comparison of three developmental root regions using secondary ion mass spectrometry imaging. Plant Physiol 112: 1289–1300
Linton RW, Goldsmith JG (1992) The role of secondary ion mass spectrometry (SIMS) in biological microanalysis: technique comparisons and prospects. Biol Cell 74:147–160
Lucas Y (2001) The role of plants in controlling rates and products of weathering: importance of biological pumping. Annu Rev Earth Planet Sci 29:135–163
Lucas Y, Luizao FJ, Chauvel A, Rouiller J, Nahon D (1993) The relation between biological activity of the rain forest and mineral composition of soils. Science 260:521–523
Ma JF, Tamai K, Yamaji N, Mitani N, Konishi S, Katsuhara M, Ishiguro M, Murata Y, Yano M (2006) A silicon transporter in rice. Nature 440:688–691. doi:10.1038/nature04590
Ma JF, Yamaji N, Mitani N, Tamai K, Konishi S, Fujiwara T, Katsuhara M, Yano M (2007) An efflux transporter of silicon in rice. Nature 448:209–212. doi:10.1038/nature05964
Martin F et al (1996) Random distribution of Ge and Si in synthetic talc: an EXAFS and FTIR study. Eur J Mineral 8:289–299
Meunier JD, Colin F, Alarcon C (1999) Biogenic silica storage in soils. Geology 27:835–838
Mitani N, Ma JF, Iwashita T (2005) Identification of the silicon form in xylem sap of rice (*Oryza sativa* L.). Plant Cell Physiol 46:279–283
Mortlock RN, Froelich PE (1987) Continental weathering of germanium: Ge/Si in the global river discharge. Geochim Cosmochim Acta 51:2075–2082
Murnane RJ, Stallard RF (1990) Germanium and silicon in rivers of the Orinoco drainage basin. Nature 344:749–752
Nikolic M, Nikolic N, Liang YC, Kirkby EA, Romheld V (2007) Germanium-68 as an adequate tracer for silicon transport in plants. Characterization of silicon uptake in different crop species. Plant Physiol 143:495–503
Perry C (2003) Silicification: the processes by which organisms capture and mineralize silica. In: Riebe P (ed)Reviews in mineralogy and geochemistry, vol 54. Mineral Society America, Washington, DC, pp 291–327
Pokrovski GS, Schott J (1998) Thermodynamic properties of aqueous Ge(IV) hydroxide complexes from 25 to 350 degrees C: implications for the behavior of germanium and the Ge/Si ratio in hydrothermal fluids. Geochim Cosmochim Acta 62(9):1631–1642
Rafi MM, Epstein E, Falk RH (1994) Silicon deprivation causes physical abnormalities in wheat (*Triticum aestivum* L.). J Plant Physiol 151:497–501
Rains DW, Epstein E, Zasoski RJ, Aslam M (2006) Active silicon uptake by wheat. Plant Soil 280:223–228
Ramseyer GO, Morrison GH (1983) Relative sensitivity factors of elements in quantitative secondary ion mass spectrometry analysis of biological reference materials. Anal Chem 55:1963–1970
Raven JA (2003) Cycling silicon—the role of accumulation in plants. New Phytol 158(3):419–421
Richmond KE, Sussmman M (2003) Got silicon? The non-essential beneficial plant nutrient. Curr Opin Plant Biol 6: 268–272
Shannon RD (1976) Revised effective ionic radii and systematic studies of interatomic distances in halides and chalcogenides. Acta Crystallogr A A32:751–767
Shannon RD, Prewitt CT (1969) Effective ionic radii in oxides and fluorides. Acta Crystallogr A B25:925–946
Tamai K, Ma JF (2003) Characterization of silicon uptake by rice roots. Plant Cell Physiol 44:43–48
Tanaka T, Homma Y, Kurosawa S (1988) Secondary ion mass spectrometric ion yields and detection limits of impurities in indium phosphide. Anal Chem 60:58–61
Treguer P, Nelson DM, Van Bennekom AJ, DeMaster DJ, Leynaert A, Queguiner B (1995) The silica balance in the world ocean: a reestimate. Science 268:375–379
White AF, Brantley SL (eds) (1995) Chemical weathering rates of silicate minerals. In: Reviews in mineralogy, vol 31. Mineralogical Society of America, Washington, DC
Wilson RG (1995) SIMS quantification in Si, GaAs, diamond—an update. Int J Mass Spectrometry 143:43–49
Yoshida S, Navasero SA, Ramirez EA (1969) Effects of silica and nitrogen supply on some leaf characters of rice plant. Plant Soil 31(1):48–56